ACS Catalysis

Letter

pubs.acs.org/acscatalysis

Cerium-Oxide-Modified Nickel as a Non-Noble Metal Catalyst for Selective Decomposition of Hydrous Hydrazine to Hydrogen

Lei He,[†,‡] Binglian Liang,[†,‡] Lin Li,[†] Xiaofeng Yang,[†] Yanqiang Huang,*[,†] Aiqin Wang,[†] Xiaodong Wang,[†] and Tao Zhang[†]

[†]State Key Laboratory of Catalysis, Dalian Institute of Chemical Physics, Chinese Academy of Sciences, 457 Zhongshan Road, Dalian 116023, China

[‡]University of Chinese Academy of Sciences, 19A Yuquan Road, Beijing 100049, China

Supporting Information

ABSTRACT: Hydrous hydrazine is identified as a hydrogen reservoir owing to its high content of hydrogen (8.0 wt %). Its selective decomposition under mild conditions is the key for quick H_2 release. Modifying Ni nanoparticles with a small amount of CeO_2 (8.0 mol %) resulted in a 3-fold increase of turnover frequency (TOF) and an enhancement of H_2 selectivity from 67% to above 99%. This improvement was due to the modification of Ni with CeO_2 nearby through strong metal−support interaction (e.g., Ni−O−Ce structure). Furthermore, this promoting effect was extended to other oxides which can form strong metal−support interaction with Ni, such as ZrO_2, MgO, and La_2O_3.

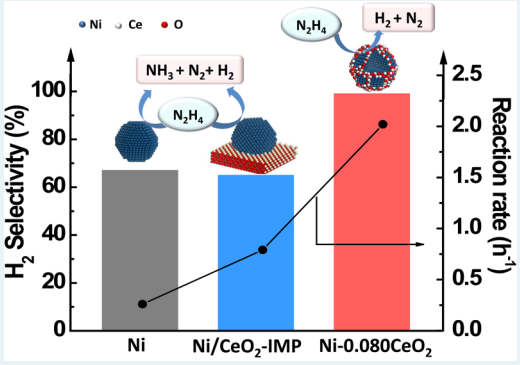

KEYWORDS: *hydrogen generation, hydrous hydrazine, non-noble metal, Ni-CeO_2, Ni−O−Ce*

There is a strong interest in using hydrous hydrazine as a hydrogen supplier in many fields, especially the unmanned space vehicles and submarine power sources where hydrazine is usually used as a propellant.[1] This is because hydrous hydrazine has the advantages of high hydrogen content (e.g., 8.0 wt % for $N_2H_4{\cdot}H_2O$), simple byproduct (N_2), and safe handling.[2] In order to obtain a high hydrogen production efficiency, the incomplete decomposition ($3N_2H_4 \rightarrow N_2(g) + 4NH_3(g)$) should be avoided. To this aim, many attempts have been made to develop an effective catalytic system to realize the selective decomposition at mild conditions. Noble-metal-modified Ni catalysts, in particular Rh−Ni,[3] Pt−Ni,[4] and Ir−Ni,[5] were most efficient for the selective decomposition of hydrous hydrazine thanks to the prominent alloy synergy effect. However, the high cost of noble metals limited their further application. Accordingly, the search for non-noble metal catalysts that are both active and selective in this reaction has received considerable attention.[6] Among various metal-based catalysts, Ni-based alloy catalysts showed 100% selectivity (e.g., Ni−Fe).[7] The general agreement on the mechanism is that the presence of the second metal altered the electronic properties of Ni and thereby facilitated the hydrogen production. In recent studies, besides the enhancement of second metallic component, nonmetal additives could also effectively promote activity and selectivity for this reaction.[8] For example, Ni−Al_2O_3 catalyst exhibited 93% selectivity due to the existence of strong basic sites provided by Al_2O_3.[9] Most recently, it has been reported that the additional amorphous Ce_2O_3 and La_2O_3 could greatly enhance the activity of NiPt or NiRh nanoparticles for H_2 generation rate.[10] However, the mechanism of the promoting effect for these oxides has not been well established.

The properties of supported catalysts are often determined by the synergy of active species (typically transition metal particles) and the supports (typically metal oxides). Sometimes, oxide supports not only play a role of dispersing active metals but also influence the metal property through geometric and electronic effect.[11] Cerium oxide (CeO_2) is the representative for such "active supports", which is considered to be able to enhance the performance of late transition metals through strong metal−support interaction.[12] For example, Au supported on CeO_2 showed higher activity and excellent stability in CO oxidation and water−gas shift (WGS) reaction due to the change of Au properties through strong interfacial bonding on CeO_2.[13] Similarly, the coprecipitated Ni/CeO_2 catalyst exhibited better catalytic performance in WGS[14] and ethanol steam reforming[15] because of the alternation of nickel's electronic property. Herein, we present a facile approach to modify Ni nanoparticles by creating metal−oxide interaction with CeO_2, through which alters the chemical properties of Ni and makes it both active and selective for hydrous hydrazine

Received: September 29, 2014
Revised: February 5, 2015
Published: February 9, 2015

DOI: 10.1021/acscatal.5b00143
ACS Catal. 2015, 5, 1623−1628

Table 1. Hydrous Hydrazine Decomposition Results for Different Catalysts at 30 °C

sample	selectivity (%)	TOF[a] (h^{-1})	reaction rate[b] ($mol_{N_2H_4}\ mol^{-1}_{Ni}\ h^{-1}$)	Ni dispersion (%)	Ni particle size[c] (nm)
Ni	67	15.0	0.26	1.74	19.8
Ni-0.005CeO_2	84	32.4	0.68	2.11	16.9
Ni-0.025CeO_2	97	41.2	2.00	4.86	12.9
Ni-0.080CeO_2	99	51.6	2.02	3.92	13.1
Ni-0.233CeO_2	99	30.5	2.05	6.74	8.7
Ni-0.500CeO_2	99	26.0	2.33	8.97	8.4
Ni/CeO_2−IMP	65	15.0	0.79	6.31	14.2

[a]TOFs were calculated on the amount of surface Ni determined by H_2 chemisorption (30% of N_2H_4 conversion). [b]Reaction rate was calculated on the amount of all the Ni in the catalyst, as reported previously.[4a] [c]Ni particle size was calculated on the basis of the XRD results, according to the Scherrer equation.

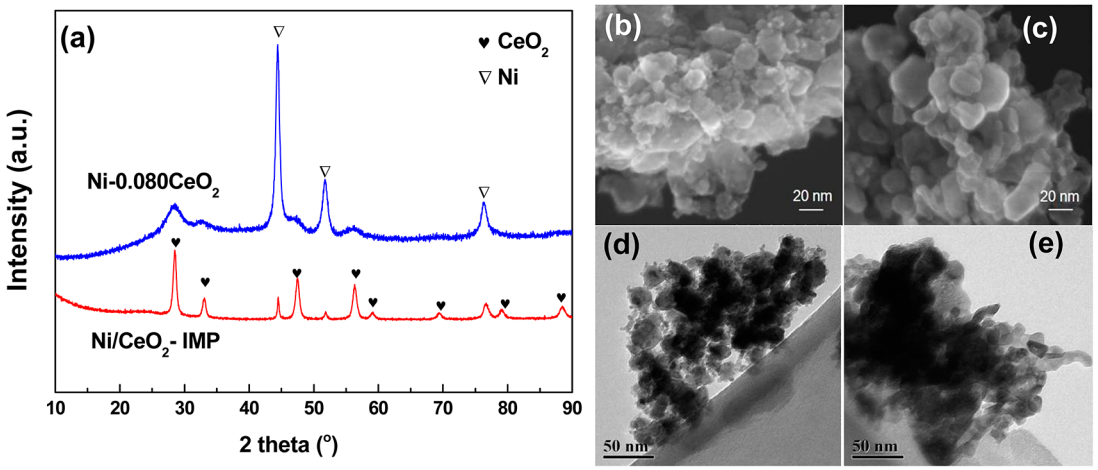

Figure 1. (a) XRD profiles for Ni-0.080CeO_2 and Ni/CeO_2−IMP; HRSEM images for the following: (b) Ni/CeO_2−IMP; (c) Ni-0.080CeO_2; and TEM images for the following: (d) Ni/CeO_2−IMP; (e) Ni-0.080CeO_2.

decomposition. The promoting effect of cerium oxide was revealed through kinetic studies and advanced characterizations.

Two types of CeO_2-modified/supported Ni catalysts were prepared by coprecipitation and impregnation methods, denoted as Ni-$x$$CeO_2$ and Ni/CeO_2−IMP, respectively (synthesis details provided in Supporting Information). Briefly, coprecipitated Ni-$x$$CeO_2$ catalysts were synthesized by adding $Ni(NO_3)_2$ and $Ce(NO_3)_3$ precursors in NaOH solution. Different amounts of cerium oxides were introduced into the Ni catalyst by varying the molar ratio of Ni and Ce precursors during the coprecipitation process. Ni/CeO_2−IMP was prepared by impregnating $Ni(NO_3)_2$ onto the CeO_2 support. The actual contents of Ni and Ce were determined by inductively coupled plasma (Table S1). In the hydrous hydrazine decomposition reaction, trace amount (n_{Ce}/n_{Ni} = 0.005) of additional CeO_2 effectively promoted H_2 selectivity from 67% to 84% (Table 1). With a further increase in the CeO_2 ratio to 0.080, H_2 selectivity surpassed 99% and remained the same at a higher CeO_2 content. In contrast, Ni/CeO_2−IMP performed only 65% selectivity for hydrogen generation, which was similar to pure Ni. In addition to the promoting of selectivity, the turnover frequency (TOF) value increased significantly after adding a small amount of CeO_2 and reached a maximum of 51.6 h^{-1} at the CeO_2 content of 0.080 (Table 1). Although there was a slight decrease of TOF values with further adjusting the CeO_2 content to 0.500, the H_2 selectivity was almost the same, suggesting similar surface properties over these coprecipitated Ni-$x$$CeO_2$ catalysts. In the recycling test, the Ni-0.080CeO_2 catalyst showed a sustainable high selectivity (above 95%) with rapid H_2 release rate after six cycles of test and remained higher than 88% after eight cycles (Figure S1a). There was not an obvious change of Ni particle size for the used catalysts according to the XRD patterns (Figure S1b). The deactivation may due to the strong adsorption of N-species or slight oxidation of Ni on the surface. The apparent activation energy (E_a) was 47.0 kJ mol^{-1}, calculated according to Arrhenius equation (Figure S1c). The H_2 selectivity maintained as high as 99% in the temperature range of 30−50 °C, although the selectivity slightly decreased to 90% when the reaction temperature further increased to 80 °C due to thermodynamic reasons, as reported elsewhere.[16] Clearly, this cerium-oxide-modified Ni is a nonexpensive and highly efficient catalyst for selective decomposition of hydrous hydrazine. Furthermore, assuming that all the Ni species participated in the reaction, as reported in the literature,[4a] the reaction rate was also calculated and listed in Table 1. The reaction rate of Ni-0.080CeO_2 was 2.02 h^{-1}, which was comparable to Ni−Pt alloy nanoparticles (1.5−7.9 h^{-1}).[4a] Therefore, Ni-0.080CeO_2 was chosen as a representative for coprecipitated sample in further characterizations.

Extended characterizations have been carried out to determine the microstructural difference between the above CeO_2-modified Ni catalysts. X-ray diffraction (XRD) patterns demonstrated the crystalline nature of freshly reduced catalysts (Figure 1a). For Ni/CeO_2−IMP, only peaks representing metallic Ni and CeO_2 phases could be detected. Beside the three peaks for Ni^0 with 2θ values of 44.5°, 51.7°, and 76.3° (PDF no. 01-087-0712), the other eight peaks could be

DOI: 10.1021/acscatal.5b00143
ACS Catal. 2015, 5, 1623−1628

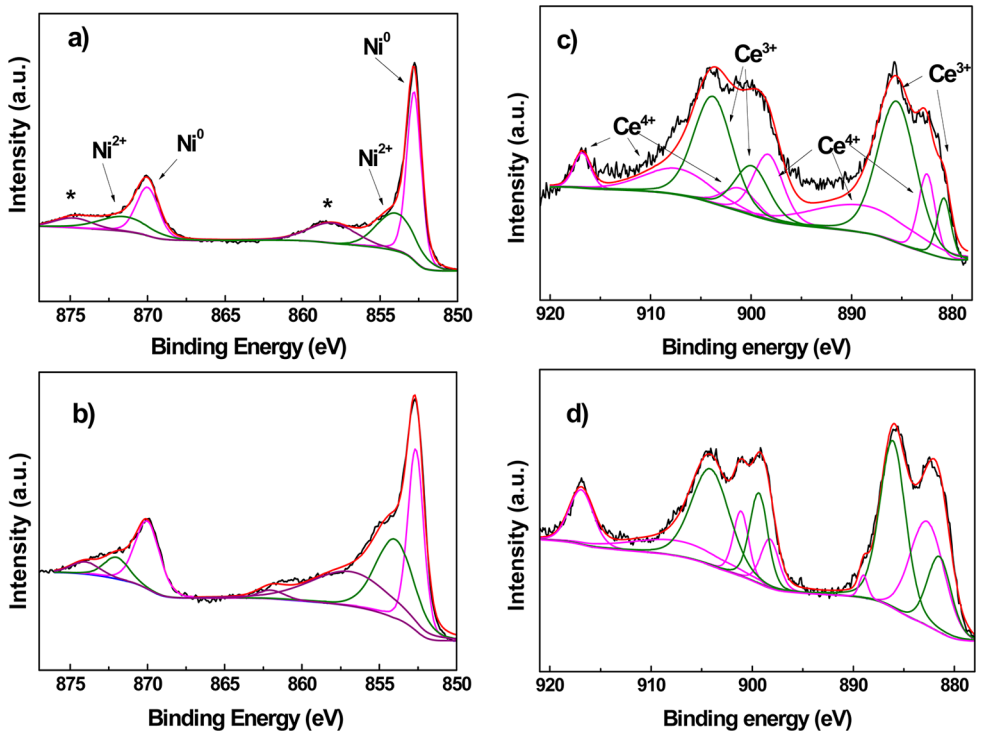

Figure 2. X-ray photoelectron spectra of the reduced Ni-0.080CeO_2 catalysts (a, c) and Ni/CeO_2−IMP catalysts (c, d): (a, b) Ni 2p; (c, d) Ce 3d.

attributed to CeO_2 with fluorite-type structure (PDF no. 00-004-0593).[17] The Ni crystalline size in this sample was 14.2 nm calculated on the basis of the Scherrer equation (Table 1). For Ni-0.080CeO_2, the main diffraction peaks represented the existence of metallic Ni. Only three weak signals could also be observed centered at 28.5°, 33.1°, and 47.5°, corresponding to the fluorite-type structured CeO_2 (PDF no. 00-004-0593). The weakened peak intensity was attributed to the low content of crystallite CeO_2. The crystallite size of Ni in Ni-0.080CeO_2 was 13.1 nm, which was comparable to Ni/CeO_2−IMP. In this case, size effect was excluded for the explanation of the selectivity and TOF difference between the above two types of catalysts. The TEM and HRSEM images (Figure 1b−e) indicated a visible structural difference between Ni-0.080CeO_2 and Ni/CeO_2−IMP. Apparently, separated Ni particles loaded on the CeO_2 support could be clearly observed on Ni/CeO_2−IMP catalyst. In contrast, Ni-0.080CeO_2 presented a uniform morphology without obvious separation of Ni and CeO_2. As the precursors for Ni and CeO_2 were atomically mixed together during coprecipitant process, the CeO_2 located closely to Ni particles in the final catalyst and resulted in a maximum interdispersion between Ni and CeO_2.[17b] Therefore, the two samples showed quite different morphologies. Although both types of catalysts mentioned above were composed of Ni and CeO_2 with similar Ni particle sizes, their catalytic performances were surprisingly distinct from each other. It suggested that the cerium oxides played a role of promoter for Ni-0.080CeO_2 instead of a traditional support to improve nickel dispersion. Therefore, more characterizations were carried out for further investigation.

A H_2-TPR experiment was employed to probe the difference in interdispersion between NiO and CeO_2 in the two types of catalysts (Figure S2). The total consumption of hydrogen and the ratio of H/Ni were summarized in Table S2. The broad H_2 consumption peak centered at 300 °C belong to the decomposition of $Ni(OH)_2$ to NiO and further reduction to metallic Ni.[18] The main H_2 consumption peaks for all the coprecipitated samples centered at 360 °C, which represented the reduction of Ni from the mixed Ni−Ce hydroxides. This reduction temperature was much higher than that for Ni/CeO_2−IMP (298 °C), indicating stronger Ni−O bonds in the precipitated samples.[18a] Notably, there was a small peak appeared at 250 °C, which could only be observed on coprecipitated Ni-$x$$CeO_2$ samples. This peak was attributed to the easy reduction of oxygen adsorbed on the vacancies of the catalysts, which originated from the incorporation of Ni^{2+} ions into the ceria lattice.[19] The H/Ni ratio was larger than 2.0 for Ni-$x$$CeO_2$ and Ni/CeO_2−IMP samples because of the partial reduction of CeO_2, which could be promoted by the spillover of H_2 from Ni nearby. The results indicated a high dispersion of Ni and CeO_2 in the coprecipitated sample, which led to a stronger interaction between them. This information was also verified by X-ray photoelectron spectroscopy (XPS) experiments (Figure 2). Ni $2p_{1/2}$ and Ni $2p_{3/2}$ regions with binding energies of 852.8 and 870.0 eV, attributed to Ni^0, were observed on both samples,[20] which coincided with the XRD results. Meanwhile, there was a small amount of NiO with the binding energy of 854.0 eV, which was due to the surface oxidation of Ni before the XPS test.[20] It is worth mentioning that the ratio of Ce^{3+}/Ce^{4+}, calculated according to the literature (Table S3),[21] for the coprecipitated Ni-0.080CeO_2 catalyst was larger than that for the impregnated sample, which indicated a stronger interaction between Ni and CeO_2 in the former sample.

We further applied Raman spectroscopy to clarify the chemical properties of CeO_2 in the obtained Ni-$x$$CeO_2$ and Ni/CeO_2−IMP catalysts (Figure 3). From the visible Raman spectra (532 nm), a peak located at 464 cm^{-1} was observed on both Ni/CeO_2−IMP and CeO_2, which featured the cubic fluorite phase of CeO_2 (F_{2g} band).[22] However, this peak

DOI: 10.1021/acscatal.5b00143
ACS Catal. 2015, 5, 1623−1628

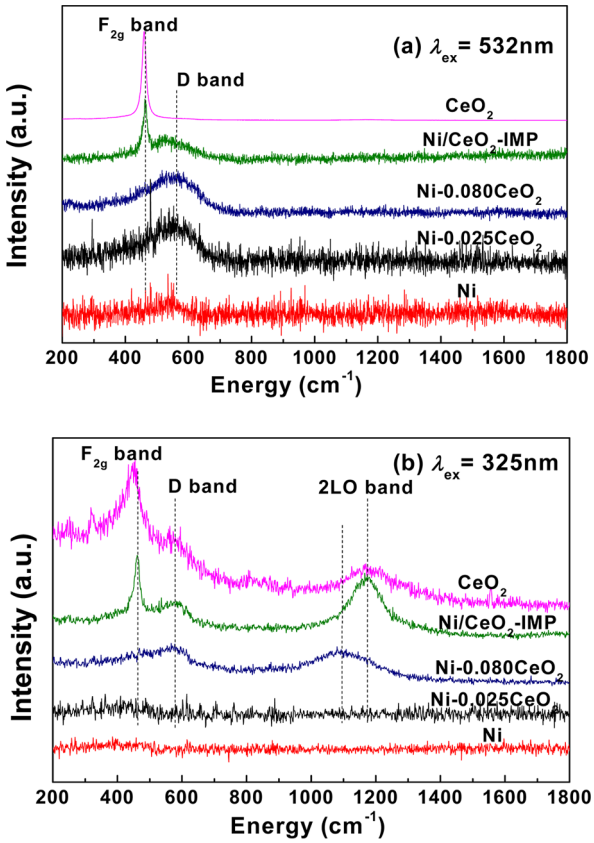

Figure 3. Visible (a) and UV (b) Raman spectra of freshly reduced Ni, CeO_2, Ni-$x$$CeO_2$, and Ni/$CeO_2$−IMP.

disappeared on the coprecipitated samples, indicating a structural destruction of fluorite CeO_2 in these samples. At the same time, a peak centered at 566 cm^{-1} was observed for Ni/CeO_2−IMP, Ni-0.080CeO_2, and Ni-0.025CeO_2 catalysts, indicating the existence of defect sites (D band).[23] The defects could be induced by two ways: (i) the oxygen vacancy originated from reducing Ce^{4+} to Ce^{3+}; (ii) the unbalanced electronic environment caused by distributing Ni into CeO_2 lattice (e.g., formation of Ni−O−Ce bond).[24] However, the stronger intensity of this peak for Ni-0.080CeO_2 indicated more oxygen vacancies due to more interaction between Ni and CeO_2 in this sample. There were no peaks observed for pure Ni due to its metallic status. We further characterized the samples using UV Raman spectra, because it is more sensitive to surface defect sites in CeO_2 due to the resonance Raman effect.[25] There was a new broad peak appeared at 1180 cm^{-1} for CeO_2, Ni/CeO_2−IMP, and Ni-0.080CeO_2, which belonged to second-order longitudinal optical mode (2LO band) of CeO_2.[24,25] This peak showed an obvious band shift to 1100 cm^{-1} on Ni-0.080CeO_2, which indicated the weakening of the Ce−O bond due to the electron transfer from Ni through the Ni−O−Ce bond.[24] Also, the peak representing fluorite phase of CeO_2 (F_{2g}) still could not be observed over the Ni-0.080CeO_2 catalyst, which further confirmed the amorphous status of CeO_2 on the surface. Combining the results of visible and UV Raman spectra, we assumed that for the coprecipitated samples, the cerium oxides existed in an amorphous form and were partially doped by Ni, which induced large amount of Ni−O−Ce bonds around the Ni particles. However, this Ni substitution in cerium oxide was very low or negligible on its impregnated counterpart due to the much lower interface area between them.

Although this Ni−O−Ce structure itself is not active for hydrous hydrazine decomposition, it could alter the chemical properties of surface Ni. This change of Ni property was probed using Fourier transform infrared (FTIR) spectroscopy of CO adsorption (Figure 4). The CO adsorption status could

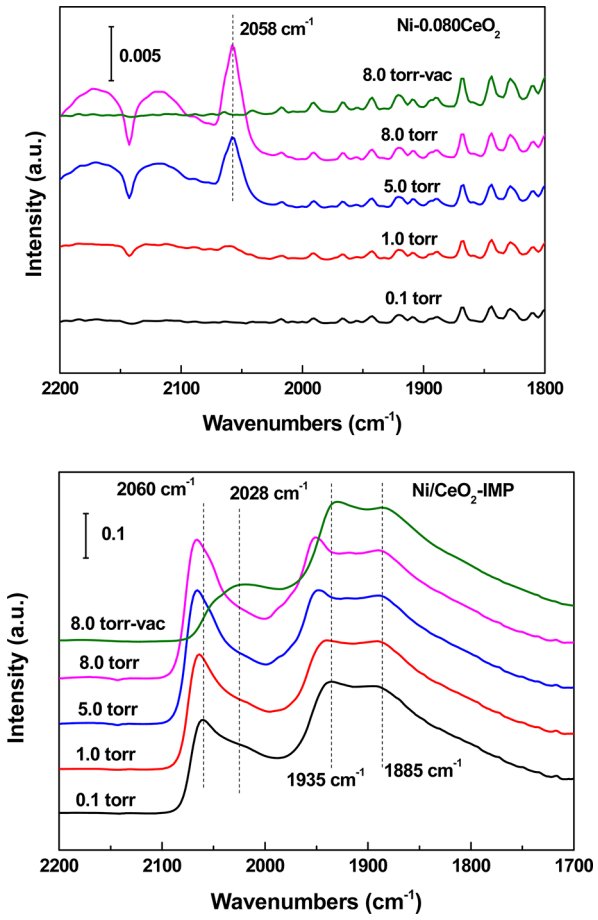

Figure 4. FT-IR spectra for CO adsorption on Ni-0.080CeO_2 and Ni/CeO_2−IMP catalysts at different equalized pressures (25 °C).

reflect the surface dispersion of Ni.[26] The intensity of the spectrum was more than 50-fold stronger on the Ni/CeO_2−IMP catalyst than that on Ni-0.080CeO_2, indicating a much weaker CO adsorption on the latter catalyst. Typically, for Ni-0.080CeO_2, there was only one weak CO adsorption peak at 2058 cm^{-1}, which did not appear until the CO pressure increased to 5.0 Torr and could be easily removed after vacuum. This peak was ascribed to nickel carbonyl species adsorbed on the highly dispersed $Ni^{\delta+}$.[27] It is an indication of the strong interaction between Ni and CeO_2. The surface Ni particle was surrounded by amorphous CeO_2, which led to an electron transfer between Ni and CeO_2 through Ni−O−Ce bond as observed in the Raman results. In contrast, there were couples of strong CO adsorption peaks observed on Ni/CeO_2−IMP catalyst. The peaks at the region of 1900−1970 cm^{-1} and 1880−1900 cm^{-1} were attributed to bridged and multicentered CO adspecies on Ni^0,[27] which were very stable and could not be removed even after vacuum. The 2028 cm^{-1} peak was attributed to linear CO adspecies on Ni^0. Also, the peak representing subcarbonyl CO adspecies on $Ni^{\delta+}$ was observed

DOI: 10.1021/acscatal.5b00143
ACS Catal. 2015, 5, 1623−1628

at 2060 cm^{-1}, which was also quite weak and disappeared after vacuum. With increasing CO pressure, all the above peaks had blue shift because of bond−bond coupling of CO molecules.[26] Results of CO adsorption experiments reflected the different surface properties of Ni on these two types of catalysts. For the coprecipitated samples, the surface Ni particle was surrounded by amorphous CeO_2, which led to an electron transfer between Ni and CeO_2 and changed the electronic properties of surface Ni. The presence of cerium oxide, even with a small amount, obviously altered the chemical properties of Ni presented in Ni-0.080CeO_2. However, in the case of Ni/CeO_2−IMP, metallic Ni particles were deposited on the CeO_2 support, which showed quite different CO adsorption compared with coprecipitated samples due to the limited interaction between Ni and CeO_2.

On the basis of the above characterization results, the structure model could be built for the highly selective and active Ni-0.080CeO_2 catalyst, as well as for its impregnated counterpart (Figure 5). For the Ni-0.080CeO_2 catalyst, the Ni

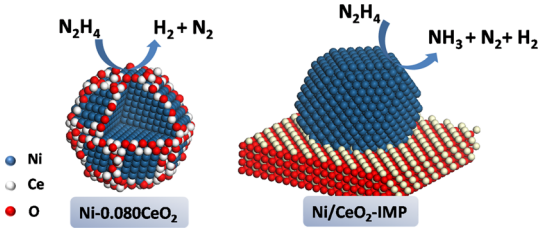

Figure 5. Structure model of Ni-0.080CeO_2 and Ni/CeO_2−IMP catalysts and the scheme of hydrous hydrazine decomposition.

particles were surrounded by amorphous CeO_2 species. The strong interaction between Ni and cerium oxide (e.g., Ni−O−Ce bonding) led to a formation of electronically perturbed Ni species ($Ni^{\delta+}$). This electronic perturbation is similar to that found in the Ni-based alloy catalysts. For the Ni−Pt catalyst,[4b] the electron transfer from Ni to Pt led to a weakened adsorption of H_2 and NH_x species on Ni particles, which resulted in a 7-fold increase of reaction rate for H_2 production. Similarly, the existence of electronic exchange between Ni and CeO_2 also altered the interaction between Ni and the N_2H_4 molecule, which facilitates N−H bond dissociation instead of N−N bond on Ni and makes the H_2 generation much easier. In other words, the additional CeO_2 played a positive role as the second metal in Ni-based bimetallic catalysts for modifying the Ni surface property in Ni-$x$$CeO_2$ catalysts. However, the intermixing between Ni and cerium oxides were less pronounced on Ni/CeO_2−IMP. Therefore, the influence of cerium oxide on Ni particles was very small or negligible on the impregnated sample, which in turn displayed comparable catalytic performance to that of pure Ni nanoparticles.

Furthermore, the strong metal−oxide interaction in the coprecipitated samples prevented the formation of fluorite structured CeO_2. Instead, amorphous CeO_2 was formed, which not only played a role of stabilizing Ni but also provided strong basic sites for this reaction. From the CO_2-TPD-MS experiments, there were large amount of strong basic sites existed on Ni-0.080CeO_2 and Ni-0.500CeO_2 catalysts (Figure S3 and Table S4), which was not observed on the impregnated catalyst. The existence of these strong basic sites may also play an important role in promoting H_2 selectivity as reported elsewhere.[7a,16] All these possible reasons made Ni-0.080CeO_2 both active and selective for H_2 generation via hydrous hydrazine decomposition. In this respect, the modifying of CeO_2 to Ni in coprecipitated samples played a critical role in improving the catalytic performance of Ni nanoparticles.

To further verify the promoting effect of oxide for the Ni catalyst, extended Ni-MO_x (M=Mg, Zr, La) catalysts were prepared by the coprecipitant method with the same Ni weight loading as Ni-0.080CeO_2 (80 wt %) and tested in the hydrous hydrazine decomposition (Table 2). These catalysts had one

Table 2. Comparison of TOF and Selectivity for Ni-MO_x (M = Mg, Zr, La) Catalysts

catalyst	metal dispersion (%)	TOF (h^{-1})	selectivity (%)
Ni-CeO_2[a]	4.0	51.6	99
Ni-ZrO_2	4.2	47.1	95
Ni-MgO	4.5	26.5	90
Ni−La_2O_3	2.5	35.9	89

[a]It refers to the Ni-0.080CeO_2 catalyst.

thing in common: the oxides chosen were easy to make a strong interaction with Ni.[28] As all these catalysts were prepared similarly with Ni-0.080CeO_2, they may provide a similar structure as the Ni-0.080CeO_2 catalyst. As expected, all of them displayed much higher TOF and H_2 selectivity (≥89%) than pure Ni nanoparticles (Table 2), demonstrating that the promoting effect of oxide could be explained not only in Ni-CeO_2 system but also for other Ni-MO_x samples, as long as the strong interaction structure can be formed between Ni and other oxides. Similar to cerium oxide, these oxides not only played a role of disperse active metal but also, more importantly, modified the electronic properties of Ni, which altered the interaction between the Ni and N_2H_4 molecule and made the H_2 generation pathway much easier.

In summary, the CeO_2-modified Ni catalysts showed a 99% H_2 selectivity and 3-fold higher TOF value than bare Ni nanoparticles for hydrous hydrazine decomposition reaction. The additional CeO_2 not only stabilized the Ni particles but also led to a strong interaction with Ni, through which the electronic property of surface Ni was modified. Besides, a large number of strong basic sites were formed as a result of the amorphous properties of CeO_2, which was also beneficial for promoting H_2 selectivity. The specific properties of Ni nanoparticles modified with CeO_2 led to a catalyst with high selectivity and TOF in hydrous hydrazine decomposition toward hydrogen generation. The promoting effect could be extended to other oxides which can form strong interaction with Ni, such as Ni-ZrO_2, Ni-MgO, and Ni−La_2O_3. This is an interesting finding and may have practical significance in designing other metal-oxide-supported catalysts with high efficiency.

■ ASSOCIATED CONTENT

Supporting Information

The following file is available free of charge on the ACS Publications website at DOI: 10.1021/acscatal.5b00143.

Experimental procedures; recycling test and Arrhenius plots for Ni-0.080CeO_2 catalyst; XPS results; H_2-TPR results; CO_2-TPD-MS results (PDF)

DOI: 10.1021/acscatal.5b00143
ACS Catal. 2015, 5, 1623−1628

AUTHOR INFORMATION

Corresponding Author

*E-mail: yqhuang@dicp.ac.cn. Fax: (+) 86-411-84685940. Tel: (+) 86-411-84379416.

Notes

The authors declare no competing financial interest.

ACKNOWLEDGMENTS

This work was supported by the National Natural Science Foundation of China (21103173, 21173218, 21203182, 21476226) and the DICP Fundamental Research Program for Clean Energy (DICPM201307).

REFERENCES

(1) (a) Schmidt, E. *Hydrazine and its derivatives: preparation, properties, applications*, 2nd ed.; John Wiley & Sons: New York, 2001, 1267−1632 ;. (b) Jiang, H.; Singh, S.; Yan, J.; Zhang, X.; Xu, Q. *ChemSusChem* **2010**, *3*, 541−549.

(2) (a) Mary, S.; Kappenstein, C.; Balcon, S.; Rossignol, S.; Gengembre, E. *Appl. Catal. A-Gen.* **1999**, *182*, 317−325. (b) Zheng, M.; Cheng, R.; Chen, X.; Li, N.; Li, L.; Wang, X.; Zhang, T. *Int. J. Hydrogen Energy* **2005**, *30*, 1081−1089. (c) Singh, S.; Zhang, X.; Xu, Q. *J. Am. Chem. Soc.* **2009**, *131*, 9894−9895.

(3) (a) Singh, S.; Xu, Q. *J. Am. Chem. Soc.* **2009**, *131*, 18032−18033. (b) Wang, J.; Zhang, X.; Wang, Z.; Wang, L.; Zhang, Y. *Energy Environ. Sci.* **2012**, *5*, 6885−6888. (c) Yoo, J.; Kim, H.; Kang, S.; Lee, B.; Hur, N. *J. Mater. Chem. A* **2014**, *2*, 18929−18937.

(4) (a) Singh, S.; Xu, Q. *Inorg. Chem.* **2010**, *49*, 6148−6152. (b) He, L.; Huang, Y.; Wang, A.; Liu, Y.; Liu, X.; Chen, X.; Delgado, J.; Wang, X.; Zhang, T. *J. Catal.* **2013**, *298*, 1−9. (c) Jiang, Y.; Kang, Q.; Zhang, J.; Dai, H.; Wang, P. *J. Power Sources* **2015**, *273*, 554−560.

(5) (a) Singh, S.; Xu, Q. *Chem. Commun.* **2010**, *46*, 6545−6547. (b) He, L.; Huang, Y.; Liu, X.; Li, L.; Wang, A.; Wang, X.; Mou, C.; Zhang, T. *Appl. Catal. B: Environ.* **2014**, *147*, 779−788.

(6) (a) Yang, F.; Li, Y.; Chu, W.; Li, C.; Tong, D. *Catal. Sci. Technol.* **2014**, *4*, 3168−3179. (b) Wang, H.; Yan, J.; Li, S.; Zhang, X.; Jiang, Q. *J. Mater. Chem. A* **2015**, *3*, 121−124.

(7) (a) Singh, S.; Singh, A.; Aranishi, K.; Xu, Q. *J. Am. Chem. Soc.* **2011**, *133*, 19638−19641. (b) Gao, W.; Li, C.; Chen, H.; Wu, M.; He, S.; Wei, M.; Evans, D.; Duan, X. *Green Chem.* **2014**, *16*, 1560. (c) Tong, D.; Tang, D.; Chu, W.; Gu, G.; Wu, P. *J. Mater. Chem. A* **2013**, *1*, 6425−6432. (d) Manukyan, K.; Cross, A.; Rouvimov, S.; Miller, J.; Mukasyan, A.; Wolf, E. *Appl. Catal. A: Gen.* **2014**, *476*, 47−53.

(8) Singh, S.; Xu, Q. *Catal. Sci. Technol.* **2013**, *3*, 1889−1900.

(9) He, L.; Huang, Y.; Wang, A.; Wang, X.; Chen, X.; Delgado, J.; Zhang, T. *Angew. Chem., Int. Ed.* **2012**, *51*, 6191−6194.

(10) (a) O, S.; Yan, J.; Wang, H.; Wang, Z.; Jiang, Q. *J. Power Sources* **2014**, *262*, 386−390. (b) Wang, H.; Yan, J.; Wang, Z.; O, S.; Jiang, Q. *J. Mater. Chem. A* **2013**, *1*, 14957−14962.

(11) (a) Bond, G.; Burch, R.; Birkett, M.; Kuhn, A. In *Catalysis*; Bond, G., Webb, G., Eds.; The Royal Society of Chemistry: London, 1983; Vol. *6*, pp 27−60. (b) Ruppert, A.; Weckhuysen, B. In *Handbook of heterogeneous catalysis*; Ertl, G., Knoezinger, H., Schuth, F., Weitkamp, J., Eds.; Wiley-VCH Verlag GmbH & Co. KGaA: Weinheim, 2008; pp 1178−1188.

(12) (a) Cargnello, M.; Doan-Nguyen, V.; Gordon, T.; Diaz, R.; Stach, E.; Gorte, R.; Fornasiero, P.; Murray, C. *Science* **2013**, *341*, 771−773. (b) Sun, C.; Li, H.; Chen, L. *Energy Environ. Sci.* **2012**, *5*, 8475. (c) Bruix, A.; Rodriguez, J.; Ramírez, P.; Senanayake, S.; Evans, J.; Park, J.; Stacchiola, D.; Liu, P.; Hrbek, J.; Illas, F. *J. Am. Chem. Soc.* **2012**, *134*, 8968−8974.

(13) (a) Ta, N.; Liu, J.; Chenna, S.; Crozier, P.; Li, Y.; Chen, A.; Shen, W. *J. Am. Chem. Soc.* **2012**, *134*, 20585−20588. (b) Park, J.; Graciani, J.; Evans, J.; Stacchiola, D.; Ma, S.; Liu, P.; Nambu, A.; Sanz, J.; Hrbek, J.; Rodriguez, J. *Proc. Natl. Acad. Sci. U. S. A.* **2009**, *106*, 4975−4980.

(14) Barrio, L.; Kubacka, A.; Zhou, G.; Estrella, M.; Martínez-Arias, A.; Hanson, J. C.; Fernández-García, M.; Rodriguez, J. *J. Phys. Chem. C* **2010**, *114*, 12689−12697.

(15) (a) Zhou, G.; Barrio, L.; Agnoli, S.; Senanayake, S.; Evans, J.; Kubacka, A.; Estrella, M.; Hanson, J.; Martínez-Arias, A.; Fernández-García, M.; Rodriguez, J. *Angew. Chem., Int. Ed.* **2010**, *49*, 9680−9684. (b) Fang, W.; Pirez, C.; Paul, S.; Capron, M.; Jobic, H.; Dumeignil, F.; Jalowiecki-Duhamel, L. *ChemCatChem.* **2013**, *5*, 2207−2216.

(16) He, L.; Huang, Y.; Wang, A.; Wang, X.; Zhang, T. *AIChE J.* **2013**, *59*, 4297−4302.

(17) (a) Pirez, C.; Capron, M.; Jobic, H.; Dumeignil, F.; Jalowiecki-Duhamel, L. *Angew. Chem., Int. Ed.* **2011**, *50*, 10193−10197. (b) Du, X.; Zhang, D.; Shi, L.; Gao, R.; Zhang, J. *J. Phys. Chem. C* **2012**, *116*, 10009−10016.

(18) (a) Roh, H.; Jun, K.; Dong, W.; Chang, J.; Park, S.; Joe, Y. *J. Mol. Catal. A: Chem.* **2002**, *181*, 137−142. (b) Li, Y.; Xie, X.; Liu, J.; Cai, M.; Rogers, J.; Shen, W. *Chem. Eng. J.* **2008**, *136*, 398−408.

(19) (a) Liao, X.; Zhang, Y.; Hill, M.; Xia, X.; Zhao, Y.; Jiang, Z. *Appl. Catal. A: Gen.* **2014**, *488*, 256−264. (b) Shan, W.; Luo, M.; Ying, P.; Shen, W.; Li, C. *Appl. Catal. A: Gen.* **2003**, *246*, 1−9.

(20) Peck, M.; Langell, M. *Chem. Mater.* **2012**, *24*, 4483−4490.

(21) Mullins, D.; Overbury, S.; Huntley, D. *Surf. Sci.* **1998**, *409*, 307−319.

(22) (a) Spanier, J.; Robinson, R.; Zhang, F.; Chan, S.; Herman, I. *Phys. Rev. B* **2001**, *64*, 245407. 1−8 (b) Lin, J.; Li, L.; Huang, Y.; Zhang, W.; Wang, X.; Wang, A.; Zhang, T. *J. Phys. Chem. C* **2011**, *115*, 16509−16517.

(23) Gamarra, D.; Munuera, G.; Hungría, A.; Fernández-García, M.; Conesa, J.; Midgley, P.; Wang, X.; Hanson, J.; Rodríguez, J.; Martínez-Arias, A. *J. Phys. Chem. C* **2007**, *111*, 11026−11038.

(24) Taniguchi, T.; Watanabe, T.; Sugiyama, N.; Subramani, A.; Wagata, H.; Matsushita, N.; Yoshimura, M. *J. Phys. Chem. C* **2009**, *113*, 19789−19793.

(25) Wu, Z.; Li, M.; Howe, J.; Meyer, H.; Overbury, S. *Langmuir* **2010**, *26*, 16595−16606.

(26) Hadjiivanov, K.; Vayssilov, G. In *Advances in Catalysis*; Academic Press: San Diego, CA, 2002; Vol. *47*, pp 307−511.

(27) (a) Poncelet, G.; Centeno, M.; Molina, R. *Appl. Catal. A: Gen.* **2005**, *288*, 232−242. (b) Jensen, M.; Morandi, S.; Prinetto, F.; Sjåstad, A.; Olsbye, U.; Ghiotti, G. *Catal. Today* **2012**, *197*, 38−49.

(28) (a) Ajayan, P.; Marks, L. *Nature* **1989**, *338*, 139−141. (b) Sánchez-Sánchez, M.; Navarro, R.; Fierro, J. *Int. J. Hydrogen Energy* **2007**, *32*, 1462−1471.

DOI: 10.1021/acscatal.5b00143
ACS Catal. 2015, 5, 1623−1628